

Harvesting Wind Energy by a Triboelectric Nanogenerator for an Intelligent High-Speed Train System

Chuguo Zhang,¹ Yuebo Liu,¹ Baofeng Zhang,¹ Ou Yang, Wei Yuan, Lixia He, Xuelian Wei, Jie Wang,* and Zhong Lin Wang*



Cite This: *ACS Energy Lett.* 2021, 6, 1490–1499



Read Online

ACCESS |



Metrics & More

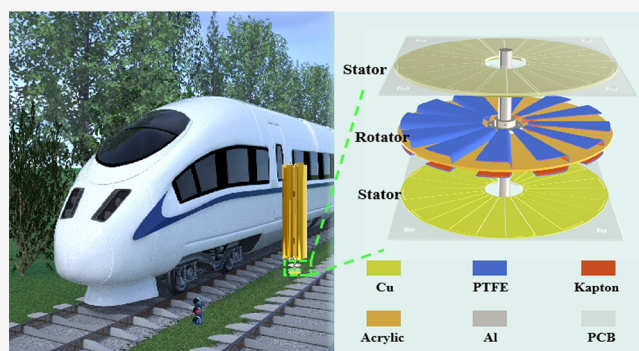


Article Recommendations



Supporting Information

ABSTRACT: The operation cost of an intelligent high-speed train system is greatly increased by the enormous energy demand of large-scale signal and sensor networks. However, the wind energy generated by high-speed trains is completely neglected. Herein, a wind-energy-harvesting device, which is based on an elastic rotation triboelectric nanogenerator (ER-TENG), is fabricated to harvest the wind energy generated by high-speed moving trains and power the relevant signal and sensing devices. Due to the significant decrease in friction force resulting from reasonable material selection and elastic structure design, the energy-harvesting efficiency of an ER-TENG is doubled and the durability is increased by 4 times compared to the same characteristics of a conventional rotation sliding triboelectric nanogenerator (RS-TENG). Our findings not only provide an *in situ* energy-harvesting pattern for an intelligent high-speed rail system by recovering the otherwise wasted wind energy generated by high-speed trains but also offer a potential strategy for large-scale wind energy harvesting by TENGs.



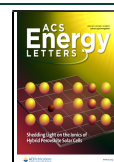
With the rapid development of high-speed rail, large-scale signal and sensor networks are being widely applied in intelligent high-speed train systems, and their huge demand for energy greatly increases the total operation cost.¹ Meanwhile, the high-voltage and large-current grid of high-speed rail systems is not suitable for powering these signal and sensor networks directly.² In addition, the requirements for extra services, such as wireless networks, real-time charging, etc., further increase the complexity and energy consumption of the whole system. Importantly, the signal and sensor networks of a railway section only function for a short time when the high-speed railway vehicles pass, while for most of the other time they are in standby mode.³ This causes a huge power loss. Therefore, a cost-effective supplement to electric power is required to solve these issues. As an alternative, a huge amount of wind energy is usually generated as high-speed railway vehicles move,⁴ but it is completely abandoned due to collection difficulties. Thus, a facile and optimized technology is needed to harvest and convert the wasted wind energy into electricity for powering the corresponding signal and sensor networks as well as service devices.

Nowadays, with their merits of light weight^{5,6} and low cost,⁷ triboelectric nanogenerators (TENGs) are regarded as one of the most effective energy-harvesting technologies to power large-scale signal and sensor networks in the Internet of things and intelligent transportation systems by *in situ* harvesting of tiny amounts of distributed energy.^{8–10} Based on the coupling of triboelectrification and electrostatic induction,^{11,12} self-powered systems composed of TENGs have been broadly used in different research fields, such as blue energy harvesting,^{13–19} high-voltage sources,^{20–22} and intelligent transportation systems.^{23,24} Conventional rotary sliding triboelectric nanogenerators (RS-TENGs) have been widely studied to harvest energy from wind^{25–28} and vehicle wheel rotation.^{29,30} However, the high pressure needed to ensure the effective contact of RS-TENGs results in many shortcomings, such as

Received: February 18, 2021

Accepted: March 22, 2021

Published: March 26, 2021



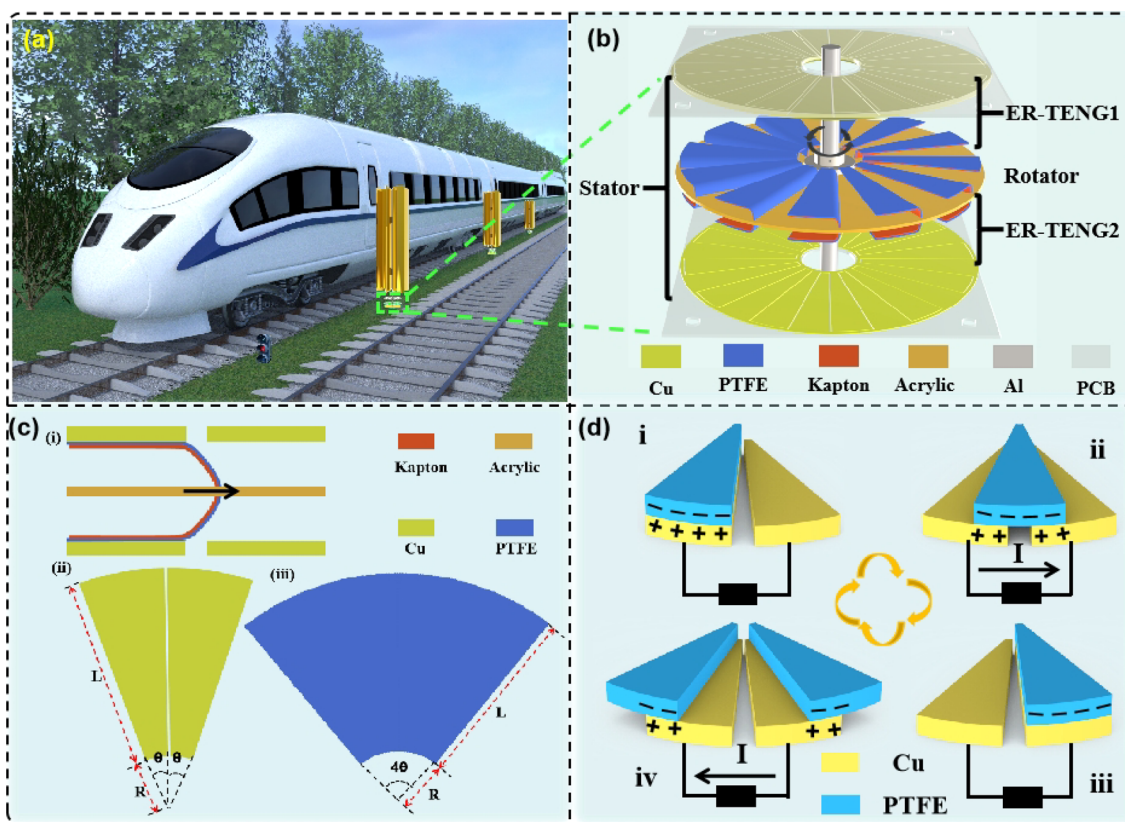


Figure 1. Structural design and working mechanism of ER-TENG. (a) Device configuration of double-layer ER-TENGs installed on both sides of the railway track at intervals. (b) Schematic representation of the structure of the double-layer ER-TENG. (c) A geometric structure design drawing of an ER-TENG. (d) The electricity generation principle of each TENG unit of the ER-TENG.

increased friction resistance, extra driving force, and easy abrasion. Therefore, the overall energy consumption and shortened life span severely impede the wide application of RS-TENGs. To overcome these, reducing the overall power consumption by lowering the frictional resistance and adding more intelligent functions to the vehicles are two important directions.

In this work, we report elastic rotation triboelectric nanogenerators (ER-TENGs) with less friction force and higher output for harvesting the otherwise wasted wind energy from the operation of high-speed rail vehicles, achieved by installing them on both sides of the railway track at intervals. Then the harvested energy can power the signal and sensing devices of a railway section. Based on the reasonable selection of dielectric materials with minimal friction coefficient, the friction force of ER-TENGs is greatly reduced. In addition, benefiting from an excellent structure design with an elastic contact mode, the driving torque of an ER-TENG is only half that of a conventional RS-TENG under the same output. Therefore, compared with the RS-TENG, the energy-harvesting efficiency of the ER-TENG is doubled. More importantly, wear is reduced owing to the significant reduction of friction, and the ER-TENG can still maintain 80% of its output performance even after 250 000 cycles of high-rotation-speed testing (200 rpm). Finally, based on perfect output performance, a double-layer ER-TENG is shown to power commercial traffic lights and sensing devices under the driving force of simulated wind, which displays the potential applications of ER-TENGs in intelligent high-speed train systems. Therefore, an ER-TENG is considered to be an effective energy-

harvesting device to power the large-scale signal and sensor networks of intelligent high-speed train systems by harvesting the otherwise wasted wind energy generated by high-speed rail vehicles.

As one of the most important modes of transportation, high-speed rail, with the advantages of high speed, punctuality, and good safety, is popular with passengers. These advantages benefit from the cooperation of large signal and sensor networks, which demand huge amounts of energy and have high operation costs. Simultaneously, the wind energy generated by the movement of high-speed rail vehicles is completely abandoned. Therefore, a cost-effective supplement to the electric power, gained by harvesting the wind energy generated by high-speed rail vehicles, is urgently needed to meet the power demands of signal and sensor networks. Here, inspired by the features of TENGs, with low cost and the ability to harvest various mechanical energy, we design a kind of double-layer elastic rotation triboelectric nanogenerator (ER-TENG) to harvest the wind energy generated by the movement of high-speed rail vehicles, which can be installed on both sides of the railway track at intervals (Figure 1a). When a high-speed train passes through a railway section, the wind energy generated will drive the ER-TENG to power the signal and sensor network, realizing a self-powered system to greatly reduce the operation cost of high-speed rail. As depicted in Figure 1b, two ER-TENGs, with 12 TENG units consisting of two printed circuit boards (PCBs) with 12 pairs of Cu electrodes in parallel connection (stator) and an acrylic board with 12 separate polytetrafluoroethylene (PTFE) and Kapton films (rotor), are integrated (stator). Coupling the stiff

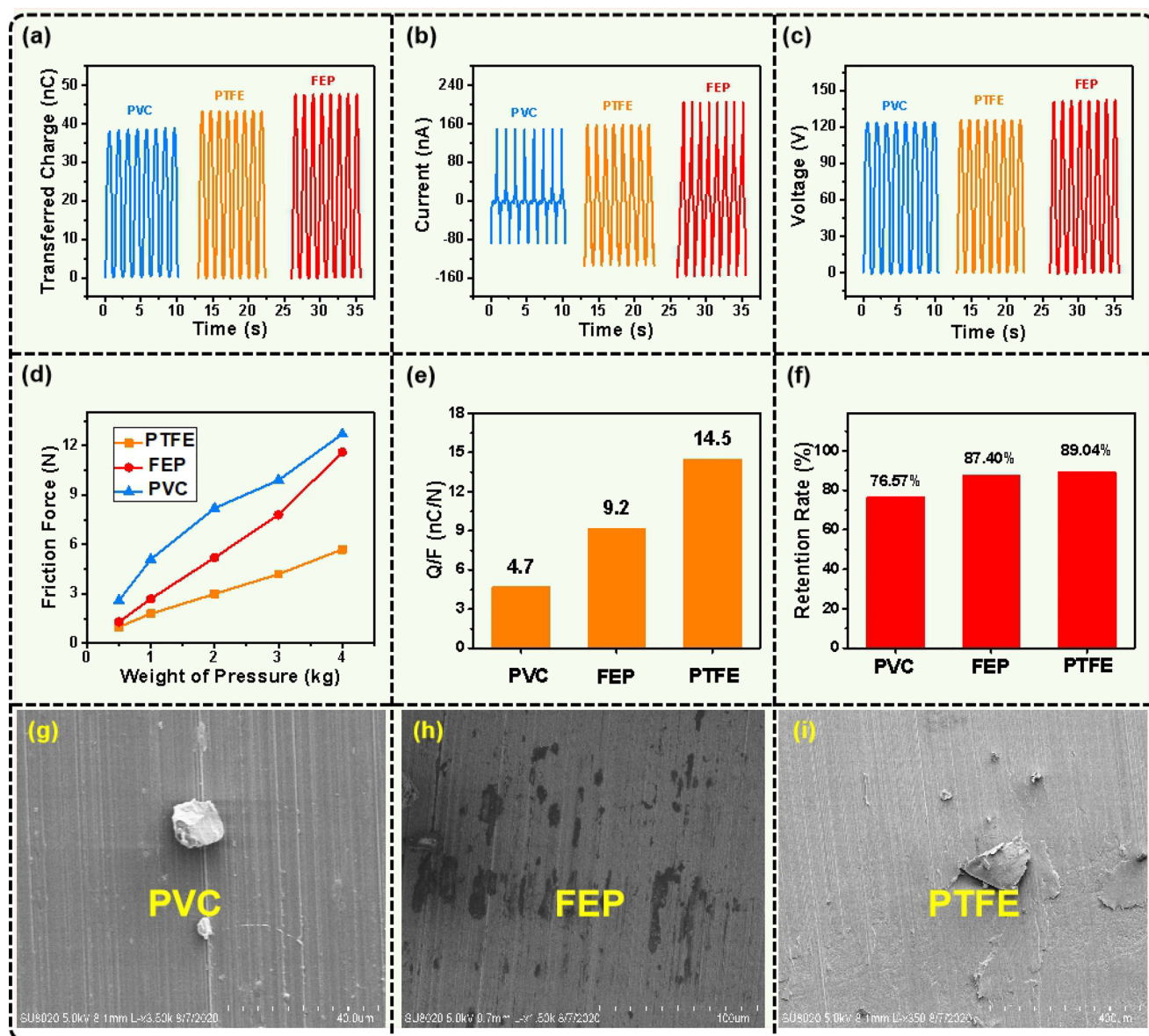


Figure 2. Output performance of three kinds of TENGs with the different dielectric materials. (a) Transferred charges, (b) short-circuit current, and (c) open-circuit voltage of three kinds of TENGs with the different dielectric materials. (d) Friction force of three kinds of TENGs under different weights. (e) Maximum transferred charges of three kinds of TENGs under unit pulling force. (f) Output performance retention rate of three kinds of TENGs after ~50 000 testing cycles. SEM images of (g) PVC film surface, (h) FEP film surface, and (i) PTFE film surface after ~50 000 testing cycles.

Kapton film on the inside and PTFE film on the outside is used to obtain a proper mechanical contact under low pressure and decrease the driving force by virtue of the low friction coefficient and low pressure. Meanwhile, the two ER-TENGs are always working in phase. The shape and size of the PTFE and Kapton films are designed by strict mathematical combination, the details of which can be found in Figure 1c and Supplementary Note 1. According to the balance of the supporting force from electrodes and elastic force from Kapton films, the ER-TENG can maintain effective contact in operation to achieve a stable output (Figures S1 and S2). Benefiting from the smaller friction coefficient of the PTFE dielectric material, the friction force of the ER-TENG will probably be reduced. In addition, good contact of the ER-TENG is achieved under low pressure based on the elastic structure, which can also significantly reduce the friction force

and thus prolong the life of the TENG by reducing the corresponding wear. Importantly, by coupling the precise combination of materials and elastic structure, a self-adaptable function is also obtained to produce a constant and high output under the operating condition of high rotation speed. Therefore, according to the above factors, the friction force is greatly reduced, and thus the ER-TENG can achieve effective energy harvesting through a small driving force and realize a longer service life. Notably, the good micro/nano structure on the surface of PTFE dielectric materials is beneficial for the improvement of the ER-TENG (Figure S3). A schematic of electricity generation by each TENG unit of the ER-TENG is displayed in Figure 1d. The PTFE dielectric film displays negative charges while the Cu electrode obtains positive charges since the electronegativity of the PTFE film is higher than that of Cu (Figure 1d-i). When the PTFE dielectric film

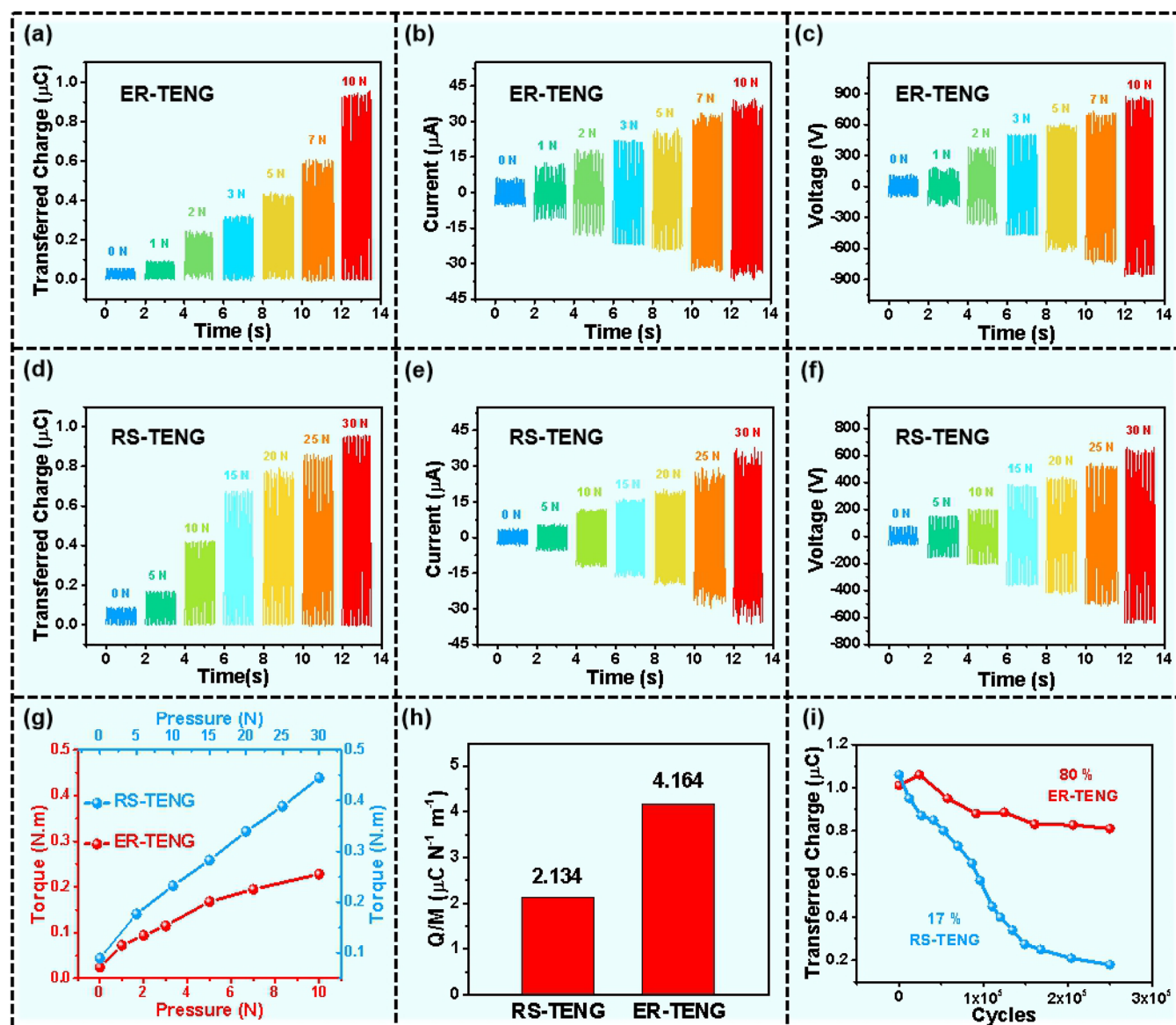


Figure 3. Performance comparison between an ER-TENG and a RS-TENG. (a) Transferred charges, (b) short-circuit current, and (c) open-circuit voltage of the ER-TENG under different pressures. (d) Transferred charges, (e) short-circuit current, and (f) open-circuit voltage of the RS-TENG under different pressures. (g) Torque of the ER-TENG and RS-TENG under different pressures. (h) Maximum transferred charges of the ER-TENG and RS-TENG under unit torque. (i) Long-term durability of the ER-TENG and RS-TENG.

slides to the right, the negative charges of PEFE dielectric film will induce the positive charges to flow from the left Cu electrode to the right one. A corresponding current is then generated (Figure 1d-ii). As the PTFE dielectric film completely coincides with the Cu electrode on the right, all the positive charges of the left Cu electrode transfer to the right one (Figure 1d-iii). Similarly, when another PEFE dielectric film reaches the left Cu electrode, the positive charge on the right Cu electrode will return to the left one, and a current occurs from right to left (Figure 1d-iv). The ideal potential distributions of ER-TENG units under different states are simulated by using COMSOL software (Figure S4 and Supplementary Note 2). As the dielectric material moves on the surface of two Cu electrodes, an electric potential distribution occurs, which shows how the alternating current is generated during the movement of the dielectric material when the two Cu electrodes are connected by an external circuit.

As one of the vital components, the dielectric materials dominate the output performance of TENG. Among to the triboelectric series of dielectric materials,³¹ polyvinyl chloride (PVC), PTFE, and fluorinated ethylene propylene (FEP) are three common dielectric materials with high output performance. However, which one is the most favorable dielectric material for ER-TENGs was still an open question. Therefore, TENGs fabricated from all three kinds of dielectric materials were designed to research their relative performance (Figure S5). As shown in Figure 2a–c, the transferred charges, short-circuit currents, and open-circuit voltages of TENGs fabricated by PVC, PTFE, and FEP are 38.5, 43, and 47.5 nC; 150, 160, and 207 nA; and 124, 126, and 141 V, respectively. It seems that all three dielectric materials are suitable for use as the triboelectric material in ER-TENGs owing to their high output performance. However, their friction properties vary a lot, as tested by using different loading masses (Figure S6). It was found that, although the friction forces of PVC, PTFE, and

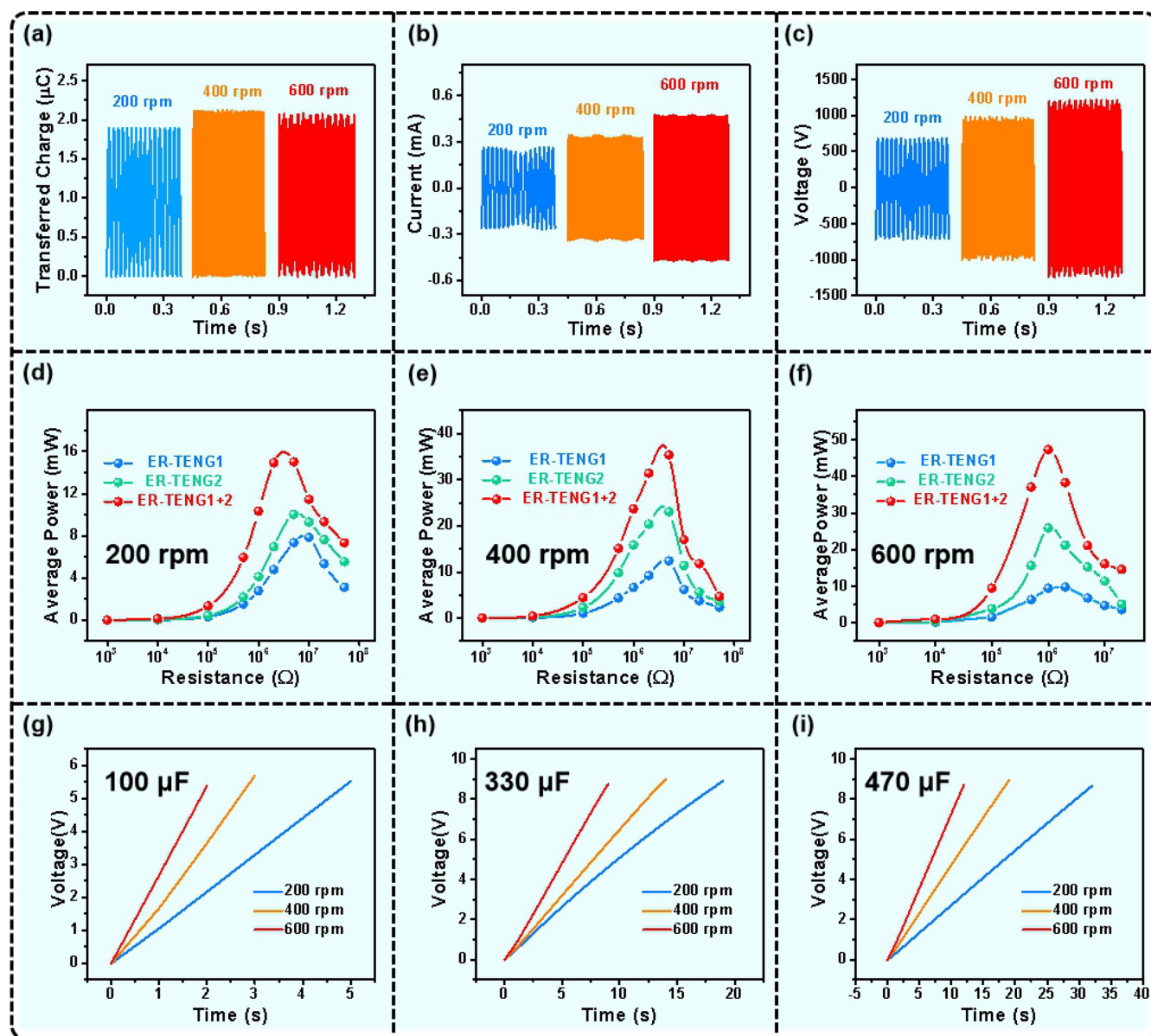


Figure 4. Output performance of the double-layer ER-TENG under different testing conditions. Top panels: (a) Transferred charges, (b) short-circuit current, and (c) open-circuit voltage of the double-layer ER-TENG with different rotation speeds of the motor. Middle panels: Average power resistance profiles of double-layer ER-TENG, ER-TENG1, and ER-TENG2 under rotation speeds of (d) 200, (e) 400, and (f) 600 rpm. Bottom panels: (g) 100 μF , (h) 330 μF , and (i) 470 μF charging of capacitors by the double-layer ER-TENG at different rotation speeds of the motor.

FEP all increase with the addition of pressure, that of the TENG fabricated by PTFE is less than those with PVC and FEP under the same pressure (Figure 2d). This result indicates that a TENG fabricated by PTFE probably requires less extra driving force, suffers reduced dielectric material wear, and minimizes mechanical energy waste. The study of transferred charges for the three kinds of TENGs under unit pulling force suggests that the TENG fabricated by PTFE transfers 1.6 times and 3 times more than the TENGs fabricated by FEP and PVC, respectively (Figure 2e and Supplementary Note 3). The output performance attenuation of the three kinds of TENGs was further studied by the corresponding retention rate of the transferred charges (Figure 2f). After about 50 000 operation cycles, the TENGs made from PVC, FEP, and PTFE maintained 76.57%, 87.4%, and 89.04% of the original outputs, respectively. SEM images (Figure 2g–i) prove that the wear

and roughness of the PTFE film surface are lower than those of PVC and FEP after 50 000 cycles. Therefore, based on comparison of the performance of three kinds of dielectric materials in sliding TENGs, PTFE is the best dielectric material for ER-TENGs because of its high output performance, low friction force, and long stability.

Although RS-TENGs made by PTFE can obtain a high output performance, high pressure is required to keep the close contact, which would result in severe abrasion and high driving force due to the increased friction force (Figure S7). Thus, keeping effective contact under low pressure is crucial for prolonging the working period of TENGs. Due to the design with an elastic structure, ER-TENGs can achieve a high output performance under a low pressure (Figure S8). Therefore, we compared the performance of a RS-TENG and an ER-TENG under different pressures. As shown in Figure 3a–c, the

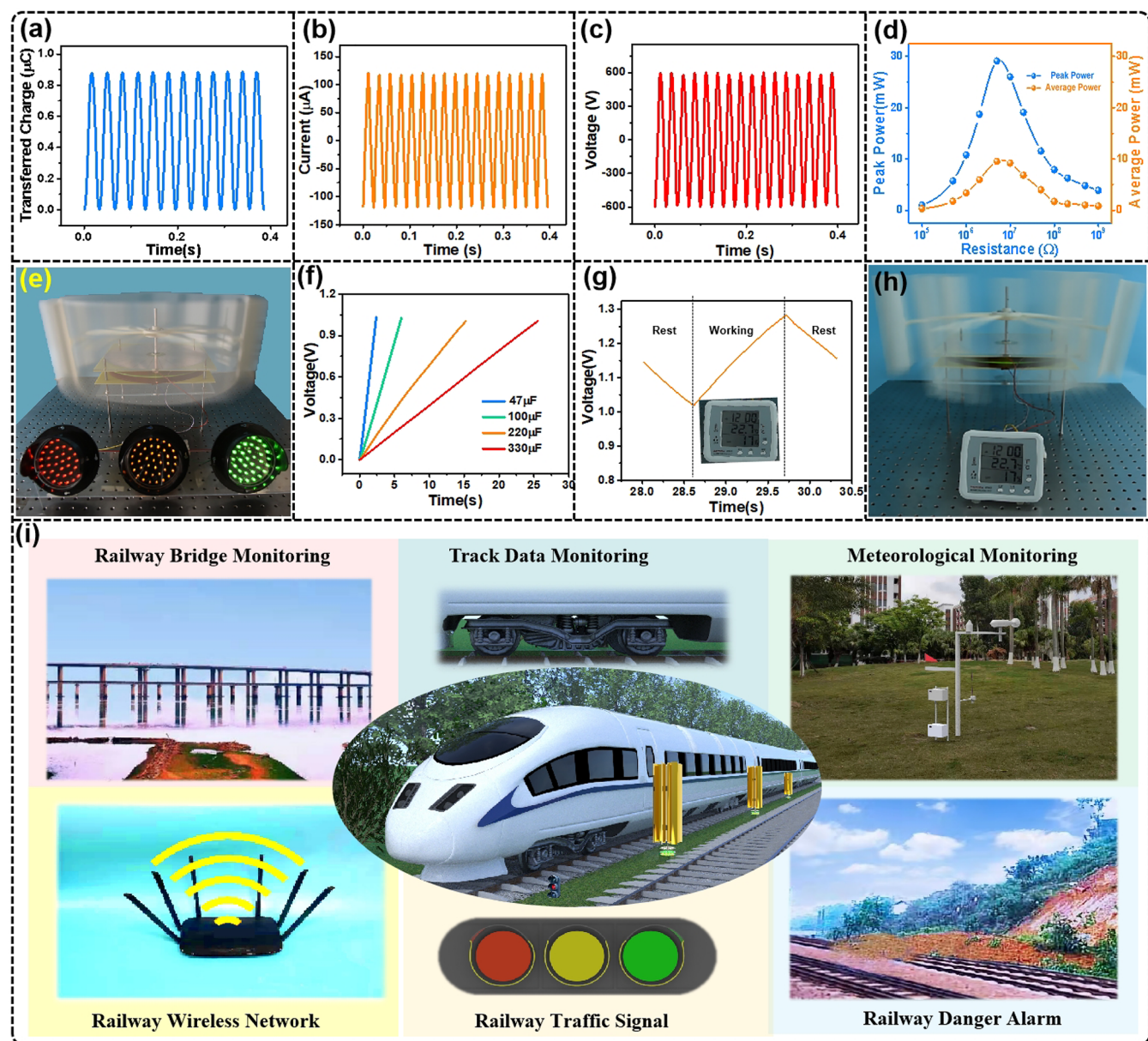


Figure 5. Application and output performance of ER-TENGs in the wind. (a) Transferred charges, (b) short-circuit current, and (c) open-circuit voltage of a double-layer ER-TENG in simulated wind. (d) Peak power and average power resistance profiles of a double-layer ER-TENG. (e) Double-layer ER-TENG as a power source for a traffic light. (f) Charging curves of 47, 100, 220, and 330 μF commercial capacitors. (g) Charging curve of the two 220 μF commercial capacitors simultaneously driving a hygrothermograph. Inset photo shows the hygrothermograph in use. (h) Photograph of a double-layer ER-TENG as a power source to drive a hygrothermograph. (i) Prospects for ER-TENGs and their application in an intelligent high-speed train system.

transferred charges, short-circuit current, and open-circuit voltage of the ER-TENG increased from 0.06 to 0.95 μC , from 5.5 to 39 μA , and from 110 to 850 V at 0 and 10 N, respectively. Meanwhile, as displayed in Figure 3c–f, the transferred charges, short-circuit current, and open-circuit voltage of the RS-TENG increased from 0.08 to 0.95 μC , from 3.5 to 37 μA , and from 70 to 640 V at 0 and 30 N, respectively. Therefore, compared with the RS-TENG, the load on the ER-TENG, with self-adaptable function due to the elastic structure, is one-third of that on RS-TENG under the same output. The main reason is that the elastic contact structure of ER-TENG allows it to achieve good contact under lower pressure, while RS-TENG has a hard contact structure and needs higher pressure to achieve effective contact. In order to

study the energy collection efficiency of the two kinds of TENGs, the corresponding driving torques of two TENGs were measured (Figure S9 and Figure 3g). It is found that, although the torques of both TENGs increase with pressure, the amount of transferred charges of the ER-TENG under unit driving torque is 2 times higher than that of the RS-TENG (Figure 3h). Therefore, the input energy for the ER-TENG is only half that of the RS-TENG, and the energy collection efficiency of the ER-TENG is doubled. More importantly, the stability of the ER-TENG was also investigated for more than 500 000 operation cycles at the high rotation speed of 200 rpm, which is based on the rotation speed of the ER-TENG in the simulated wind. The transferred charge output of the ER-TENG compared with that of the conventional RS-TENG

demonstrated that ER-TENG exhibits remarkable long-term durability, maintaining 80% electric output after 250 000 operation cycles, while the electric output of the conventional RS-TENG sharply declines to 17% after only 30 000 cycles (Figure 3i). The reason for this is that the ER-TENG has less friction torque than the conventional RS-TENG. These advantages indicate that ER-TENGs have the advantages of less driving force, higher energy collection efficiency, and longer durability than RS-TENGs.

To improve the power output and optimize the structure design, we fabricated a double-layer ER-TENG, composed of the upper ER-TENG1 and the lower ER-TENG2 in parallel (Figure 1b). It features many distinct advantages: (1) excellent triboelectrification performance of PTFE to ensure high output performance; (2) elastic structure design to keep good contact effectiveness and achieve a higher output performance and higher energy-harvesting efficiency under a lower driving torque; (3) less pressure needed by the elastic structure to reduce the friction torque and improve the durability of double-layer ER-TENG. As depicted in Figure 4a–c, a transferred charge as high as 2.2 μC can be realized. In addition, the short-circuit current increases from 0.26 to 0.48 mA with increasing rotation speed from 200 to 600 rpm, and the open-circuit voltage follows the same trend from 690 V (200 rpm) to 1200 V (600 rpm). The root-mean-square (RMS) value of the short-circuit current increases from 0.16 to 0.35 mA with rotation speeds from 200 to 600 rpm, and the RMS value of the open-circuit voltage increases from 450 to 725 V, accordingly (Supplementary Note 4). Because the double-layer ER-TENG consists of ER-TENG1 and ER-TENG2, the output performance of the individual ER-TENGs, displayed in Figures S10 and S11, indicates that the transferred charges and short-circuit current of the double-layer ER-TENG are the sums of the upper (ER-TENG1) and lower RS-TENG (ER-TENG2) owing to the simultaneous phase states during the working process. In addition, we find that the output performance of ER-TENG2 is slightly higher than that of ER-TENG1. The reason is that the ER-TENG2 is in the lower part, which has a larger pressure and better contact due to the effect of gravity on the rotor itself. Figure 4d–f shows the average power-resistance profiles of ER-TENG1, ER-TENG2, and double-layer ER-TENG, which indicates that the highest average power of double-layer ER-TENG increases from 15 to 47 mW with the change in the rotation speed of the rotating motor from 200 to 600 rpm. Meanwhile, the peak power-resistance profiles of ER-TENG1, ER-TENG2, and double-layer ER-TENG presented in Figure S12 show that the peak power of double-layer ER-TENG increases from 54 to 114 mW with the change in the rotation speed of the rotating motor from 200 to 600 rpm. It is obvious that the power of double-layer ER-TENG is equal to the sum of the power of ER-TENG1 and ER-TENG2. In addition, to further measure the output performance for practical application, the double-layer ER-TENG under various rotation speeds was used to charge the capacitors of 100, 330, and 470 μF , respectively (Figure 4g–i). Following the circuit diagram shown in Figure S13, it takes double-layer ER-TENG 2, 3, and 5 s, respectively, to charge the capacitor of 100 μF from 0 to 5.5 V at rotation speeds of 200, 400, and 600 rpm. Compared with the charging curves of ER-TENG1 and lower ER-TENG2 displayed in Figures S14 and S15 and the circuit diagram presented in Figure S16, the double-layer ER-TENG composed of ER-TENG1 and lower ER-TENG2 can charge the capacitor faster

under the same conditions. Therefore, benefiting from the higher output performance, the ER-TENG can effectively harvest the wind energy generated by high-speed trains. Finally, we research the output performance of the ER-TENG under different humidity and temperature (the rotation speed is 60 rpm), which are two important factors that affect the output performance of TENGs. The output performance of ER-TENG decreased with increasing humidity and temperature (Figures S17–S19). The relative reasons are that the adsorption of water molecules on the surface of dielectric materials and the hot electron emission of electrons on the surface of dielectric materials will reduce the surface charge density of the dielectric materials.^{32,33} These issues will be addressed by surface modification in future work.³⁴

As a kind of device that converts rotating mechanical energy into electrical energy, the ER-TENG needs the assistance of a wind blade to realize the collection of wind energy. Therefore, to better demonstrate the application of ER-TENGs in intelligent high-speed train systems, we fabricated a windmill with vertical blades to combine with the double-layer ER-TENG (Figure S20) to harvest the wind energy generated by high-speed trains. In the relevant research, the wind speed of our simulated wind field was about 20 m s^{-1} , which is far less than the stable wind speed of 100 m s^{-1} generated by the high-speed railway. Therefore, the ER-TENG can be expected to generate higher output performance in the wind generated by the high-speed railway. Under the driving force of simulated wind (Figure 5a–c), the transferred charges, short-circuit current, and open-circuit voltage of our double-layer ER-TENG are 0.9 μC , 120 μA , and 600 V, respectively. Meanwhile, the double-layer ER-TENG can achieve RMS values of current and voltage of 68 μA and 370 V, respectively. The output power of the double-layer ER-TENG, as shown in Figure 5d, shows that the peak power and average power are 29.1 mW and 9.5 mW, respectively, at a loading resistance of 50 $\text{M}\Omega$. As displayed in Figure 5e and Movie S1, the double-layer ER-TENG can power a set of traffic lights composed of red, yellow, and green LED arrays (total power 6 W) by harvesting the wind energy using the corresponding circuit depicted in Figure S21. As a wind-energy-harvesting device, the double-layer ER-TENG generates electricity that can also be stored in capacitors or batteries to power functional electronic devices. For harvested wind energy, the charging curves of different capacitors charged by the double-layer ER-TENG are displayed in Figure 5f, and the detailed circuit is shown in Figure S13. It takes only 2.5, 6.0, 15, and 25.5 s to charge 47, 100, 220, and 330 μF capacitors to 1.0 V, respectively. More importantly, as a wind energy harvester, the double-layer ER-TENG can power the sensors and the energy storage device simultaneously. A self-powered railway environment monitoring system is achieved by integrating a double-layer ER-TENG with two commercial capacitors (220 μF) in series (energy storage device) and a commercial hygromicrothermograph (sensors) as depicted in Figure S22. The voltage of the two commercial capacitors is monitored by a potentiostat at different double-layer ER-TENG working conditions, as shown in Figure 5g. Initially, the voltage of the two commercial capacitors (220 μF) in series decreases by powering the commercial hygromicrothermograph when the double-layer ER-TENG is not connected to the circuit. Then the voltage of the two commercial capacitors (220 μF) in series increases when the double-layer ER-TENG starts to work, driven by the wind. This suggests that double-layer ER-TENGs can not only offset

the consumption of power by the commercial hygrothermograph but also charge the two commercial capacitors (220 μF) in series. However, as the double-layer ER-TENG stops operating, the voltage of the two commercial capacitors (220 μF) in series is reduced due to the consumption by the commercial hygrothermograph. The inset photograph in Figure 5g depicts the commercial hygrothermograph in the working stage. According to the advantages of the excellent harvesting ability of double-layer ER-TENGs for wind energy, a double-layer ER-TENG can directly drive sensing devices (for example, a hygrothermograph) without any assistance from electronic device components; this is demonstrated in Figure 5h and Movie S2, and the related circuit is presented in Figure S22. The installation of double-layer ER-TENGs along a railway section, which are used to harvest the wind energy generated by the high-speed train *in situ* as it passes through the railway section and can directly power small signal devices or sensing devices in the related railway section to work for a short time, shows great potential for application in intelligent high-speed train systems (Figure 5i). First, the double-layer ER-TENGs can power the sensor networks of railway bridge monitoring,³⁵ track data monitoring,³⁶ and railway meteorological monitoring when installed in the specific railway sections. Second, they can drive the hazard alarm devices and signal devices to ensure the safe and stable operation of the railway system. Finally, double-layer ER-TENGs would simplify the function of the existing high-speed rail vehicles and reduce the energy consumption of the vehicles. For example, the double-layer ER-TENGs can supply power for wireless networks and other devices, and they can be installed on both sides of the track rather than on the high-speed trains to meet the requirements of passengers. Therefore, based on their low cost, higher energy-harvesting efficiency, and longer service life, double-layer ER-TENGs can supply power for large-scale high-speed railway signal and sensor networks. Their use also provides a potential strategy for the future construction of an intelligent high-speed railway system.

In summary, an elastic rotation triboelectric nanogenerator (ER-TENG), which can be installed on both sides of the track, is designed to harvest wind energy generated by high-speed rail to power signal devices and sensing devices *in situ*. The reasonable selection of the dielectric material for the ER-TENG and the design using an elastic structure are conducive to reduce the friction force and wear of TENGs and improve their energy efficiency and durability. Therefore, compared with conventional RS-TENGs, the energy-harvesting efficiency of ER-TENGs is doubled, and the durability of ER-TENGs is increased by a factor of 4. Furthermore, ER-TENGs offer the advantages of simple fabrication, low cost, and higher energy-harvesting efficiency, and a double-layer ER-TENG can power commercial traffic lights and sensing devices driven by simulated wind, displaying the significant potential applications of ER-TENGs in an intelligent high-speed train system. In a word, this work provides a potential strategy for the construction of an intelligent high-speed railway system in the future. More importantly, the relative research offers an idea for the large-scale development of a distributed energy resource.

■ ASSOCIATED CONTENT

SI Supporting Information

The Supporting Information is available free of charge at <https://pubs.acs.org/doi/10.1021/acsenerylett.1c00368>.

Supplementary Notes 1–4, providing the dimensional design of the PTFE geometry, the parameter condition of the ER-TENG unit in different states by COMSOL simulation, the relationship between the transferred charges of unit tension and energy-harvesting efficiency, and the relationship between the peak value and RMS values; Figures S1–S16, providing a stress analysis diagram of the electrification layer of an elastic structure, a real photograph of the electrification layer of an elastic structure, a SEM image of the PTFE surface, the electric potential distribution of the ER-TENG unit under different states by COMSOL simulation, a device diagram of TENG for dielectric material selection, a schematic diagram of the TENG friction force test, structure diagrams of RS-TENG and ER-TENG, a schematic diagram of the torque test, the output performance of ER-TENG1 and ER-TENG2 under different rotation speeds, the peak power of double-layer ER-TENG, ERTENG1, and ER-TENG2 under different test conditions, the corresponding circuit diagram of double-layer ER-TENG to charge capacitors, charging curves of capacitors by the ER-TENG1 and by the lower ER-TENG2 under different rotation speeds of the motor, the corresponding circuit diagram of ER-TENG to charge capacitors, the transferred charge of ER-TENG under different humidity and temperature, the short-circuit current of ER-TENG under different humidity and temperature, the open-circuit voltage of ER-TENG under different humidity and temperature, a photograph of double-layer ER-TENG with the driving windmill, the corresponding circuit diagram of double-layer ER-TENG to light the traffic lights, and the corresponding circuit diagram of double-layer ER-TENG to drive hygrothermograph (PDF)

Video S1: A set of traffic lights are lighted by harvesting the wind energy of double-layer ER-TENG (MP4)

Video S2: A hygrothermograph is driven by harvesting the wind energy of a double-layer ER-TENG (MP4)

■ AUTHOR INFORMATION

Corresponding Authors

Jie Wang – Beijing Institute of Nanoenergy and Nanosystems, Chinese Academy of Sciences, Beijing 100083, P. R. China; College of Nanoscience and Technology, University of Chinese Academy of Sciences, Beijing 100049, P. R. China; Center on Nanoenergy Research, School of Physical Science and Technology, Guangxi University, Nanning 530004, P. R. China; orcid.org/0000-0003-4470-6171; Email: wangjie@binn.cas.cn

Zhong Lin Wang – Beijing Institute of Nanoenergy and Nanosystems, Chinese Academy of Sciences, Beijing 100083, P. R. China; School of Materials Science and Engineering, Georgia Institute of Technology, Atlanta, Georgia 30332, United States; Email: zhong.wang@mse.gatech.edu

Authors

Chuguo Zhang – Beijing Institute of Nanoenergy and Nanosystems, Chinese Academy of Sciences, Beijing 100083, P. R. China; College of Nanoscience and Technology, University of Chinese Academy of Sciences, Beijing 100049, P. R. China

Yuebo Liu – Beijing Institute of Nanoenergy and Nanosystems, Chinese Academy of Sciences, Beijing 100083, P. R. China;

Center on Nanoenergy Research, School of Physical Science and Technology, Guangxi University, Nanning 530004, P. R. China

Baofeng Zhang – Beijing Institute of Nanoenergy and Nanosystems, Chinese Academy of Sciences, Beijing 100083, P. R. China; College of Nanoscience and Technology, University of Chinese Academy of Sciences, Beijing 100049, P. R. China

Ou Yang – Beijing Institute of Nanoenergy and Nanosystems, Chinese Academy of Sciences, Beijing 100083, P. R. China; College of Nanoscience and Technology, University of Chinese Academy of Sciences, Beijing 100049, P. R. China

Wei Yuan – Beijing Institute of Nanoenergy and Nanosystems, Chinese Academy of Sciences, Beijing 100083, P. R. China; College of Nanoscience and Technology, University of Chinese Academy of Sciences, Beijing 100049, P. R. China

Lixia He – Beijing Institute of Nanoenergy and Nanosystems, Chinese Academy of Sciences, Beijing 100083, P. R. China; College of Nanoscience and Technology, University of Chinese Academy of Sciences, Beijing 100049, P. R. China

Xuelian Wei – Beijing Institute of Nanoenergy and Nanosystems, Chinese Academy of Sciences, Beijing 100083, P. R. China; College of Nanoscience and Technology, University of Chinese Academy of Sciences, Beijing 100049, P. R. China

Complete contact information is available at:

<https://pubs.acs.org/10.1021/acsenerylett.1c00368>

Author Contributions

[†]C.Z., Y.L., and B.Z. contributed equally to this work.

Notes

The authors declare no competing financial interest.

ACKNOWLEDGMENTS

This research was supported by the National Key R&D Project from the Minister of Science and Technology (2016YFA-0202701), the National Natural Science Foundation of China (Grant Nos. 61774016, 21773009, 51432005, 5151101243, and 51561145021), the China Postdoctoral Science Foundation (2019M660587), and the Beijing Municipal Science & Technology Commission (Z171100000317001, Z1711000-02017017, and Y3993113DF). The authors also thank Haining Yu for assistance with this work.

REFERENCES

- (1) Lederman, G.; Chen, S. H.; Garrett, J. H.; Kovacevic, J.; Noh, H. Y.; Bielak, J. Track Monitoring from the Dynamic Response of A Passing Train: A Sparse Approach. *Mech. Syst. Signal Process.* **2017**, *90*, 141–153.
- (2) Zhu, G.; Yang, W.; Zhang, T.; Jing, Q.; Chen, J.; Zhou, Y. S.; Bai, P.; Wang, Z. L. Self-Powered, Ultrasensitive, Flexible Tactile Sensors Based on Contact Electrification. *Nano Lett.* **2014**, *14*, 3208–3213.
- (3) Zhang, B.; Chen, J.; Jin, L.; Deng, W.; Zhang, L.; Zhang, H.; Zhu, M.; Yang, W.; Wang, Z. L. Rotating-Disk-Based Hybridized Electromagnetic-Triboelectric Nanogenerator for Sustainably Powering Wireless Traffic Volume Sensors. *ACS Nano* **2016**, *10*, 6241–6247.
- (4) Bian, Y.; Jiang, T.; Xiao, T.; Gong, W.; Cao, X.; Wang, Z.; Wang, Z. L. Triboelectric Nanogenerator Tree for Harvesting Wind Energy and Illuminating in Subway Tunnel. *Adv. Mater. Technol.* **2018**, *3*, 1700317.
- (5) Wang, J.; Li, X.; Zi, Y.; Wang, S.; Li, Z.; Zheng, L.; Yi, F.; Li, S.; Wang, Z. L. A Flexible Fiber-Based Supercapacitor-Triboelectric-

Nanogenerator Power System for Wearable Electronics. *Adv. Mater.* **2015**, *27*, 4830–4836.

(6) Chun, S.; Choi, Y.; Son, W.; Jung, J.; Lee, S.; Kim, H.; Pang, C.; Park, W.; Kim, J. High-Output and Bending-Tolerant Triboelectric Nanogenerator Based on an Interlocked Array of Surface-Functionalized Indium Tin Oxide Nanohelices. *ACS Energy Lett.* **2019**, *4*, 1748–1754.

(7) Dong, K.; Peng, X.; An, J.; Wang, A. C.; Luo, J.; Sun, B.; Wang, J.; Wang, Z. L. Shape Adaptable and Highly Resilient 3D Braided Triboelectric Nanogenerators as E-Textiles for Power and Sensing. *Nat. Commun.* **2020**, *11*, 2868.

(8) Zhang, B.; Wu, Z.; Lin, Z.; Guo, H.; Chun, F.; Yang, W.; Wang, Z. L. All-in-one 3D Acceleration Sensor Based on Coded Liquid-Metal Triboelectric Nanogenerator for Vehicle Restraint System. *Mater. Today* **2020**, *10*, 003.

(9) Guo, H.; Pu, X.; Chen, J.; Meng, Y.; Yeh, M.-H.; Liu, G.; Tang, Q.; Chen, B.; Liu, D.; Qi, S.; Wu, C.; Hu, C.; Wang, J.; Wang, Z. L. A Highly Sensitive, Self-Powered Triboelectric Auditory Sensor for Social Robotics and Hearing Aids. *Sci. Robot.* **2018**, *3*, No. eaat2516.

(10) Zhang, C.; Liu, L.; Zhou, L.; Yin, X.; Wei, X.; Hu, Y.; Liu, Y.; Chen, S.; Wang, J.; Wang, Z. L. Self-Powered Sensor for Quantifying Ocean Surface Water Waves Based on Triboelectric Nanogenerator. *ACS Nano* **2020**, *14*, 7092–7100.

(11) Zhao, Z.; Dai, Y.; Liu, D.; Zhou, L.; Li, S.; Wang, Z. L.; Wang, J. Rationally Patterned Electrode of Direct-Current Triboelectric Nanogenerators for Ultrahigh Effective Surface Charge Density. *Nat. Commun.* **2020**, *11*, 6186.

(12) Zhou, L.; Liu, D.; Zhao, Z.; Li, S.; Liu, Y.; Liu, L.; Gao, Y.; Wang, Z. L.; Wang, J. Simultaneously Enhancing Power Density and Durability of Sliding-Mode Triboelectric Nanogenerator via Interface Liquid Lubrication. *Adv. Energy Mater.* **2020**, *10*, 2002920.

(13) Liang, X.; Jiang, T.; Liu, G.; Feng, Y.; Zhang, C.; Wang, Z. L. Spherical Triboelectric Nanogenerator Integrated with Power Management Module for Harvesting Multidirectional Water Wave Energy. *Energy Environ. Sci.* **2020**, *13*, 277–285.

(14) Wang, H.; Xu, L.; Bai, Y.; Wang, Z. L. Pumping up the Charge Density of a Triboelectric Nanogenerator by Charge-Shuttling. *Nat. Commun.* **2020**, *11*, 4203.

(15) Zhang, C.; Zhou, L.; Cheng, P.; Liu, D.; Zhang, C.; Li, X.; Li, S.; Wang, J.; Wang, Z. L. Bifilar-Pendulum-Assisted Multilayer-Structured Triboelectric Nanogenerators for Wave Energy Harvesting. *Adv. Energy Mater.* **2021**, 2003616.

(16) Leung, S.; Fu, H.; Zhang, M.; Hassan, A.; Jiang, T.; Salama, K.; Wang, Z. L.; He, J. Blue Energy Fuels: Converting Ocean Wave Energy to Carbon-Based Liquid Fuels via CO₂ Reduction. *Energy Environ. Sci.* **2020**, *13*, 1300–1308.

(17) Xu, W.; Zheng, H.; Liu, Y.; Zhou, X.; Zhang, C.; Song, Y.; Deng, X.; Leung, M.; Yang, Z.; Xu, R. X.; Wang, Z. L.; Zeng, X.; Wang, Z. *Nature* **2020**, *578*, 392–396.

(18) Wang, Z. L. New Wave Power. *Nature* **2017**, *542*, 159–160.

(19) Zhang, C.; Zhao, Z.; Yang, O.; Yuan, W.; Zhou, L.; Yin, X.; Liu, L.; Li, Y.; Wang, Z. L.; Wang, J. Bionic-fin-structured Triboelectric Nanogenerators for Undersea Energy Harvesting. *Adv. Mater. Technol.* **2020**, *5*, 2000531.

(20) Li, A.; Zi, Y.; Guo, H.; Wang, Z. L.; Fernández, F. M. Triboelectric Nanogenerators for Sensitive Nano-coulomb Molecular Mass Spectrometry. *Nat. Nanotechnol.* **2017**, *12*, 481–487.

(21) Li, Y.; Bouza, M.; Wu, C.; Guo, H.; Huang, D.; Doron, G.; Temenoff, J. S.; Stecenko, A.; Wang, Z. L.; Fernández, F. M. Sub-nanoliter Metabolomics via Mass Spectrometry to Characterize Volume-Limited Samples. *Nat. Commun.* **2020**, *11*, 5625.

(22) Cheng, J.; Ding, W.; Zi, Y.; Lu, Y.; Ji, L.; Liu, F.; Wu, C.; Wang, Z. L. Triboelectric Microplasma Powered by Mechanical Stimuli. *Nat. Commun.* **2018**, *9*, 3733.

(23) Jin, L.; Deng, W.; Su, Y.; Xu, Z.; Meng, H.; Wang, B.; Zhang, H.; Zhang, B.; Zhang, L.; Xiao, X.; Zhu, M.; Yang, W. Self-Powered Wireless Smart Sensor Based on Maglev Porous Nanogenerator for Train Monitoring System. *Nano Energy* **2017**, *38*, 185–192.

(24) Yang, H.; Pang, Y.; Bu, T.; Liu, W.; Luo, J.; Jiang, D.; Zhang, C.; Wang, Z. L. Triboelectric Micromotors Actuated by Ultralow Frequency Mechanical Stimuli. *Nat. Commun.* **2019**, *10*, 2309.

(25) Ren, Z.; Wang, Z.; Liu, Z.; Wang, L.; Guo, H.; Li, L.; Li, S.; Chen, X.; Tang, W.; Wang, Z. L. Energy Harvesting from Breeze Wind ($0.7\text{--}6\text{ m s}^{-1}$) Using Ultra-Stretchable Triboelectric Nanogenerator. *Adv. Energy Mater.* **2020**, *10*, 2001770.

(26) Han, S.; Lee, E.; Kim, B.; Jung, S.; Jeong, S.; Kim, S.; Choi, Y.; Lee, S. High-Performance Dual-Mode Triboelectric Nanogenerator Based on Hierarchical Auxetic Structure. *ACS Energy Lett.* **2020**, *5*, 3507–3513.

(27) Han, K.; Luo, J.; Feng, Y.; Xu, L.; Tang, W.; Wang, Z. L. Self-Powered Electrocatalytic Ammonia Synthesis Directly from Air as Driven by Dual Triboelectric Nanogenerators. *Energy Environ. Sci.* **2020**, *13*, 2450–2458.

(28) Han, K.; Luo, J.; Feng, Y.; Lai, Q.; Bai, Y.; Tang, W.; Wang, Z. L. Wind-Driven Radial-Engine-Shaped Triboelectric Nanogenerators for Self-Powered Absorption and Degradation of NO_x. *ACS Nano* **2020**, *14*, 2751–2759.

(29) Wang, J.; Meng, C.; Gu, Q.; Tseng, M. C.; Tang, S. T.; Kwok, H. S.; Cheng, J.; Zi, Y. Normally Transparent Tribo-Induced Smart Window. *ACS Nano* **2020**, *14*, 3630–3639.

(30) Xie, Z.; Zeng, Z.; Wang, Y.; Yang, W.; Xu, Y.; Lu, X.; Cheng, T.; Zhao, H.; Wang, Z. L. Novel Sweep-Type Triboelectric Nanogenerator Utilizing Single Freewheel for Random Triggering Motion Energy Harvesting and Driver Habits Monitoring. *Nano Energy* **2020**, *68*, 2211.

(31) Zou, H.; Zhang, Y.; Guo, L.; Wang, P.; He, X.; Dai, G.; Zheng, H.; Chen, C.; Wang, A. C.; Xu, C.; Wang, Z. L. Quantifying the Triboelectric Series. *Nat. Commun.* **2019**, *10*, 1427.

(32) Bui, V.; Oh, J.; Kim, J.; Zhou, Q.; Huynh, D.; Oh, I. Nest-Inspired Nanosponge-Cu Woven Mesh Hybrid for Ultrastable and High-Power Triboelectric Nanogenerator. *Nano Energy* **2020**, *71*, 104561.

(33) Xia, X.; Wang, H.; Guo, H.; Xu, C.; Zi, Y. On the Material-Dependent Charge Transfer Mechanism of the Contact Electrification. *Nano Energy* **2020**, *78*, 105343.

(34) Wen, R.; Guo, J.; Yu, A.; Zhai, J.; Wang, Z. L. Humidity-Resistive Triboelectric Nanogenerator Fabricated Using Metal Organic Framework Composite. *Adv. Funct. Mater.* **2019**, *29*, 1807655.

(35) Li, S.; Liu, D.; Zhao, Z.; Zhou, L.; Yin, X.; Li, X.; Gao, Y.; Zhang, C.; Zhang, Q.; Wang, J.; Wang, Z. L. A Fully Self-Powered Vibration Monitoring System Driven by Dual-Mode Triboelectric Nanogenerators. *ACS Nano* **2020**, *14*, 2475–2482.

(36) Wang, L.; Zhang, Y.; Lie, S. T. Detection of Damaged Supports under Railway Track Based on Frequency Shift. *J. Sound Vib.* **2017**, *392*, 142–153.